APPENDIX A

Numerical Groundwater Flow and Contaminant Transport Model
SFPP Mission Valley Terminal
San Diego, California

APPENDIX A TABLE OF CONTENTS

A-1.0 INTRODUCTION A-1
A-1.1 Geologic Setting A-2
A-1.2 Previous Model A-3
A-1.3 Horizontal Resolution A-4
A-1.4 Vertical Resolution A-4
A-1.5 Model Grid and Layering/Stratigraphy A-5
A-1.6 Boundary Conditions A-7
A-1.7 Additional Features A-8

A-2.0 HYDROSTRATIGRAPHY A-9
A-2.1 Geologic Indicator Kriging A-9
A-2.2 Geologic Log Data Input A-9
A-2.3 Description of GIK Gridding A-10
A-2.4 Indicator Kriging Parameters and Settings A-10
A-2.4.1 Mapping GIK Results to the DYN Computational Grid A-12
A-2.4.2 Observations and Comparisons A-12

A-3.0 MODEL SIMULATIONS A-13
A-3.1 Calibration A-13
A-3.2 Calibrated Hydraulic Properties A-14
A-3.3 Validation A-15
A-3.4 Mass Balance A-16
A-3.5 Transport Modeling A-16
A-3.5.1 DYNTRACK Program A-16
A-3.5.2 Transport Modeling Approach A-17
A-3.5.3 Transport Modeling Results A-20
A-3.6 Sensitivity Analysis A-21
A-3.7 Numerical Mass Flux calculations A-22
A-3.8 Hypothetical Municipal Well Simulation A-23

A-4.0 CONCLUSIONS AND RECOMMENDATIONS A-24

A-5.0 REFERENCES A-25

TABLES (in text)

A-1 Geology of the MVT Vicinity
A-2 Summary of Recharge Parameters
A-3 Geologic Indicator Kriging Material Assignments
A-4 Baseline Modeled Hydraulic Properties
A-5 Summary of Water Mass Balance
A-6 Parameter Values Related to Dispersion

FIGURES

A-1 Geology of the MVT Vicinity
A-2 Old and New Model Domain and Finite Element Grid
A-3 Aerial Photograph of Mission Valley Texture-Mapped onto Topography
A-4 Aerial Photograph and DYN Grid
A-5 Elevation Contours of the Top of the Friars Formation
A-6 Model Domain and Boundary Conditions
A-7 Locations of Stormwater Drains and Sewers
A-8 Recharge Distribution Showing the Effects of Pavement, Irrigation, and Mesa-Front Recharge
A-9 DYN Grid with Borings
A-10 Opaque Texture-Mapped Aerial Photograph with Soil Borings
A-11 Convex Hull with Soil Boring Locations used for GIK
A-12 GIK Results Interpolated into DYN Model – Friars Formation Only
A-13 GIK Results Interpolated into DYN Model – Friars Formation + High K Alluvium Only
A-14 GIK Results Interpolated into DYN Model – Friars Formation + High K + Medium K Alluvium Only
A-15 GIK Results Interpolated into DYN Model – Friars Formation + High K + Medium K + Low K Alluvium Only
A-16 GIK Results Interpolated into DYN Model – Friars Formation + All Alluvium
A-17 GIK Results Interpolated into DYN Model Layers 1 through 2
A-18 GIK Results Interpolated into DYN Model Layers 1 through 3

A-19 GIK Results Interpolated into DYN Model Layers 1 through 4

A-20 GIK Results Interpolated into DYN Model Layers 1 through 5

A-21 GIK Results Interpolated into DYN Model Layers 1 through 6

A-22 Material Properties Assigned to Elements in Layer 2

A-23 Transect 1 Showing Interpolated Aquifer Materials

A-24 Observed and Simulated Recovery at Well R-32

A-25 Observed and Simulated Recovery at Well R-34

A-26 Hydrograph – Wells in Murphy Canyon

A-27 Hydrograph – Wells in the Pumping Capture Zone

A-28 Hydrograph – Wells Near the San Diego River

A-29 Calibration Plot for High Water Level Event (2/2003)

A-30 Calibration Plot for Low Water Level Event (8/2002)

A-31 Calibration to Low Water Levels in August 2002 – Differences in Water Levels with 5 Wells Pumping

A-32 Calibration to Low Water Levels in August 2002 – Differences in Water Levels in Shallow Alluvium

A-33 Calibration to High Water Levels in February 2003 – Differences in Water Levels with 7 Wells Pumping

A-34 Calibration to High Water Levels in February 2003 – Differences in Water Levels in Shallow Alluvium

A-35 Cross-section with Velocity Vectors Near the San Diego River – Upward Gradients Below and to the South of the River

A-36 Particle Track and Travel Time after Release into the Steady-State, No Pumping Scenario

A-37 Mass Flux Comparison of Empirical and Numerical Calculations

A-38 Empirical and Numerical comparison of total plume mass

A-39 Groundwater Elevation Contours for Pumping Under 2002 Pumping Scenario – Five Recovery Wells Pumping a Total of 182 gpm

A-40 Groundwater Elevation Contours for Pumping Under 2003 Pumping Scenario – Seven Recovery Wells Pumping a Total of 165 gpm

A-41 Observed and Simulated MTBE Distribution in May 2001

A-42 Observed and Simulated MTBE Distribution in 2003

A-43 Simulated MTBE Distribution in 2010

A-44 Groundwater Elevation Contours in 2010 for a Hypothetical Production Well Pumping at 200 gpm

A-45 Simulated Concentration of MTBE in a Hypothetical Production Well at R-26

CERTIFICATION

All hydrogeologic and geologic information, conclusions, and recommendations in this document have been prepared under the supervision of and reviewed by an LFR Levine·Fricke California Registered Geologist.

Eric Rogoff 1/30/04

Eric Rogoff, R.G., C.E.G. Date
Senior Associate Hydrogeologist
California Registered Geologist #5658
California Registered Engineering Geologist #1776

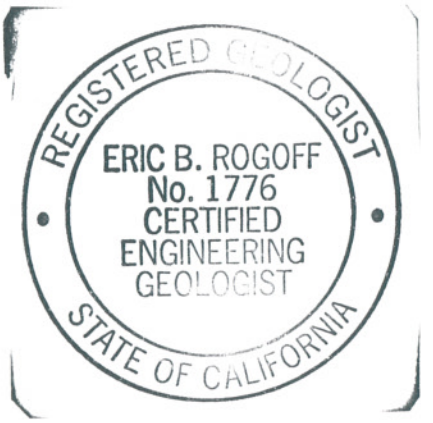

All engineering information, conclusions, and recommendations in this document have been prepared under the supervision of and reviewed by an LFR Levine·Fricke California Professional Engineer.

Jan 30, 2004

Eric M. Nichols, P.E. Date
Principal Engineer and Vice President
California Professional Engineer C42695

* A registered geologist's and/or professional engineer's certification of conditions comprises a declaration of his or her professional judgment. It does not constitute a warranty or guarantee, expressed or implied, nor does it relieve any other party of its responsibility to abide by contract documents, applicable codes, standards, regulations, and ordinances.

A-1.0 INTRODUCTION

This document presents the methodologies, results, and conclusions of the Groundwater Flow and Contaminant Transport Modeling at the Mission Valley Terminal on behalf of SFPP, L.P., operating partner of Kinder Morgan Energy Partners (Kinder Morgan). This work was performed in accordance with the "Groundwater and Contaminant Transport Model Work Plan" (LFR 2002), which was submitted in fulfillment of Task B.1 of Time Schedule Order (TSO) No. R9-2002-0042 adopted by the California Regional Water Quality Control Board, San Diego Region (RWQCB) on March 13, 2002.

This groundwater model was built upon a previous finite element DYNFLOW groundwater flow model, constructed for the site in 1999 (CDM 1999b). The previous groundwater model was updated and refined to better represent site conditions and to improve confidence in its use as a predictive tool. Contaminant transport was simulated with DYNTRACK, a companion code to DYNFLOW that can model three-dimensional contaminant transport for constituents subject to adsorption, dispersion, and first-order transformation. DYNTRACK is used to predict the variation in time and space of a release of dissolved chemical. The method implemented is the Lagrangian approach, which uses a random-walk technique whereby a statistically significant number of particles are tracked through the groundwater flow domain. Each particle represents a discrete parcel of solute mass which, when divided into the water volume of an element-cell, specifies the concentration at that time and location.

The scope of work outlined in the "Work Plan for Groundwater and Contaminant Transport Modeling" included the following objectives:

- use of the contaminant transport model to estimate the dissolved mass flux of methyl tertiary-butyl ether (MTBE) at two transects, including a transect downgradient of recovery wells RW-3A through RW-7, and a transect south of recovery well RW-9
- projection of the time required to attain water-quality objectives (e.g., drinking water standards in a hypothetical municipal well) consistent with designated beneficial uses downgradient from the containment system, and estimation of exposure point concentrations to known or reasonably anticipated future receptors

In order to accomplish these objectives, the Work Plan identified the following tasks:

- expansion of the model domain south of the San Diego River to include the full width of the Mission Valley alluvium
- incorporation of additional geologic information interpreted from geologic logs completed after the groundwater flow model was created in 1999 (TRC 2000; Kleinfelder 2000, 2001a, 2001b, 2002a, 2002b; LFR 2002b, 2003d)
- refinement of the vertical resolution of the groundwater flow model based upon well clusters installed since 1999

- representation of hydrostratigraphic interpretations by permeability zones correlated to geologic logs using geostatistical methods
- recalibration of the groundwater flow model with updated water level data in both steady-state and transient conditions
- incorporation of more detailed drainage and recharge data
- development and calibration of a contaminant transport model
- use of the contaminant transport model to estimate the dissolved mass flux of MTBE at two transects, including a transect downgradient of recovery wells RW-3A through RW-7, and a transect south of recovery well RW-9
- projection of the time required to attain water-quality objectives (e.g., drinking water standards in a hypothetical municipal well) consistent with designated beneficial uses downgradient from the containment system, and estimation of exposure point concentrations to known or reasonably anticipated future receptors

Work was performed in a manner consistent with the following references and guidance standards:

- "Standard Guide for Application of a Ground-Water Flow Model to a Site-Specific Problem," American Society for Testing and Materials (ASTM) D5447-93
- "Standard Guide for Comparing Ground-Water Flow Model Simulations to Site-Specific Information," ASTM D5490-93
- "Standard Guide for Documenting a Ground-Water Flow Model Application," ASTM D5718-95 (Reapproved 2000)
- "Standard Guide for Calibrating a Ground-Water Flow Model Application," ASTM D5981-96
- "Ground Water Modeling for Hydrogeologic Characterization – Vol. 1 Field Investigation Manual," California EPA, July 1995
- "Compilation of Ground-Water Models," U.S. EPA 1993, EPA/600/R-93/118. Including references to 3-dimensional flow: DYNFLOW (#4990) and solute transport: DYNTRACK (#4941)

A-1.1 Geologic Setting

The finite-element model domain consists primarily of permeable Holocene alluvium deposited in channels historically cut by Murphy Creek and the San Diego River into relatively impermeable Pleistocene and Tertiary bedrock formations. Figure A-1 illustrates the alluvial deposits and the surrounding bedrock formations. The geologic units, listed stratigraphically downward, are summarized in Table A-1.

Table A-1: Geology of the MVT Vicinity

Period	Epoch	Unit	Description
Quaternary	Holocene	Alluvium and Slopewash	unconsolidated clay, silt, sand, and gravel
	Pleistocene	Stream-Terrace Deposits	unconsolidated sand and gravel
		Lindavista Formation	sandstone, conglomerate
Tertiary	Eocene	Mission Valley Formation	sandstone
		Stadium Conglomerate	cobble conglomerate
		Friars Formation	sandstone, claystone
		Scripps Formation	sandstone, conglomerate
Cretaceous	Upper Cretaceous	Rosario Group	sandstone, conglomerate

Source: California Dept. of Conservation, 2001.

The bedrock formations were considered impermeable in setting the boundaries for the previous model domain (CDM 1999b) where the Friars Formation underlying the alluvium was simulated as a no-flow boundary. In the current revised model, the upper portion of the Friars Formation beneath the alluvium was assigned a relatively low hydraulic conductivity value (Section A-3.2) because some weathering has been observed in the upper portion of the Friars Formation. Relatively low concentrations of MTBE (typically <20 micrograms per liter [µg/l]) have also been detected in deep monitoring wells R-21FS, R-25FS, and R-28FS, suggesting that localized upper portion of the Friars Formation may be hydraulically communicating with the deeper alluvium. However, cross-contamination during well installation is suspected as the reason MTBE is present in these wells.

A-1.2 Previous Model

The previous model assumed a steady-state flow field and was calibrated to water levels from the 1997 period. At the time the original model was calibrated, there were limited temporal and vertical water level data downgradient from extraction wells RW-1 through RW-7. With significantly more data being available since 1999, the model was updated and revised to increase horizontal and vertical resolution, and to incorporate accumulated pumping data, revised estimates of recharge rates, and observed trends in water quality and water levels. These data were used to revise initial conditions, boundary conditions, and calibration targets in a manner consistent with ASTM standard guides (1993b, 1996a).

A-1.3 Horizontal Resolution

The previous model domain (CDM 1999b) extended from Murphy Canyon to the San Diego River, covering only the north side of the San Diego River flood plain. In 2001, three multi-level monitoring well nests (R-23, R-28, and R-31) were installed south of the river. Data from these wells were incorporated into the model to span the full width of Mission Valley with the model domain, allowing an improved representation of the total water balance. The previous and revised model domains are illustrated on Figure A-2. The model domain was chosen in such a way as to most accurately describe boundary conditions along its borders in a manner consistent with Wang and Anderson (1982). Physical boundaries such as outcrops and streams have been used to delineate the model domain. Outcrops form impervious boundaries along the northern and southern edge of the model. The elements that pinch out against the outcrops are often very thin and/or unsaturated. However, they were included in this model because they do contribute aerial recharge. The east and west bounds are transects drawn perpendicular to San Diego River Valley with sufficient distance from remedial pumping not to affect calibration results. At the northern end of Murphy Canyon, the saturated aquifer is very thin (<5 feet); instead of extending the domain further into this box canyon, a no-flow boundary was specified. Water was brought into the model in the upper reach of Murphy Canyon Creek using a river boundary condition along the creek. The contacts between the alluvium and terrace deposits and the consolidated deposits of the deeply incised Mission Valley canyon (Figure A-1) provided ideal locations to specify boundary conditions along the perimeter of the model domain. Figure A-3, which is an aerial photograph texture-mapped onto topographic data, illustrates the relief of the hills, Mission Valley, and Murphy Canyon. Figure A-4 shows a plan view of the updated model grid superimposed on an aerial photograph and a map of site features.

After the southern portion of the San Diego River Flood plain was added in the model, a new computational mesh was created and new boundary conditions were assigned and calibrated. New nodes and elements were added within the existing domain to increase resolution near wells, landscaping irrigation areas, potentially leaking storm-water or sewer conveyance lines, and other water fluxes. Landscape irrigation areas include the stadium field, trees within the stadium parking lot, the practice field, and areas irrigated along roadways. The model encompasses the entire area that may be hydraulically influenced by remedial pumping, and provides a more transparent water balance than the 1999 model, in which the San Diego River was represented as a no-flow boundary. The expansion of the model domain allows modeling of groundwater withdrawals near the river and transport of contaminants beneath and across the river. The extent of the model domain is sufficiently large to allow the model to serve potential future uses as a water resource management tool for Mission Valley.

A-1.4 Vertical Resolution

The previous model consisted of three layers. In 1999, fewer hydrogeologic data were available, so there was not sufficient vertical geological or hydrostratigraphic data to justify detailed vertical discretization. The three layers were obtained by dividing the interval

between the bedrock and the land surface into three equally spaced layers. The local topographic changes caused by the stadium structure were represented only in the top layer, to prevent obvious man-made distortions of the underlying layers. Uniform average hydraulic properties were assigned over the vertical extent of the model because the available hydraulic property data at the time of model calibration had been collected across the entire thickness of the alluvium. This representation was satisfactory for defining general rates and directions of groundwater flow in the aquifer.

From 1999 to the present, 26 nested monitoring wells have been installed (TRC 2000; Kleinfelder 2000, 2001a, 2001b, 2002a, 2002b; LFR 2002b, 2002f, 2003b). The nested wells generally are screened in intervals designated shallow alluvium (AD), middle alluvium (AM), deep alluvium (AD), and shallow Friars Formation (FS). Monitoring data from these nested wells suggest that as groundwater flows downgradient from the residual light nonaqueous phase liquid (LNAPL) zone, MTBE concentrations generally decrease. In some well nests, MTBE concentrations are greater in wells screened within the middle intervals than in the shallow and deeper intervals. The data from the nested wells drilled since 1999 have been used to significantly modify the previous model to allow a more detailed representation of the hydrostratigraphy.

A-1.5 Model Grid and Layering/Stratigraphy

The number of model layers was increased from 3 to 7. The number of computational nodes in three dimensions was increased from 8,436 in the previous model to 25,144 in the current model. The total number of elements (cells) was increased from 12,474 to 42,441. These modifications were performed to improve model predictions regarding resolution of flow paths, extent of hydraulic capture, and the extent of solute migration and attenuation. The most evident change to the model is the inclusion of the southern portion of the San Diego River flood plain. The northern boundary has also been slightly extended to coincide with the terrace outcrop observed in the aerial photographs texture-wrapped onto topography. This extends the domain surface area to 2.1 square miles from the original 1.2 square miles. Another modification includes the assignment of material classes, based on interpretations of geologic logs, to individual model cells and layers. The current model uses seven material layers, where the bottom layer represents the upper portion of the Friars Formation. The upper portion of the Friars Formation is represented as conductive layer with a uniform thickness of 25 feet. The previous model ended at the bottom of the alluvium, representing the contact of the alluvium and the Friars Formation as a no-flow boundary.

Within each layer, the number of nodes in the finite element mesh is 3,143, which form 6,063 triangular elements in each layer. Within seven layers, the model space is discretized by 42,441 material cells. Each cell is assigned one of five types of material properties, as generated by geologic indicator kriging. The selected indicator is based on a grouping of material types as encountered in boreholes. The soil group symbols (indicators) have been classified as follows:

- High conductivity alluvium (poorly graded sands, SP; well-graded gravels, GW; silty gravels, GM; and clayey gravels, GC)
- Medium conductivity alluvium (clayey sands, SC; silty sands, SM)
- Low conductivity alluvium (low plasticity clays, CL; high plasticity clays, CH; low plasticity silts, SM)
- Very low permeability in the consolidated Friars Formation
- Uniform conditions in the primarily unsaturated fill materials overlying the alluvium in some locations

The indicator kriging was applied to the region between the underlying Friars Formation and the overlying unsaturated overburden. Uniform material properties were assigned to the Friars Formation and to the unsaturated overburden. Overburden has not been described in the logs of many of the boreholes, or it has been recorded simply as "fill." Because this material is unsaturated and plays no role in a groundwater flow except in transmitting recharge, a uniform Medium conductivity soil property was assigned to it. The land surface topography has been retrieved from digitized aerial photographs with 2-foot resolution (City of San Diego, 2002). Because of this fine detail, the top layer reflects features such as bridge ramps, berms, and stadium structure. The model top layer is mostly unsaturated and these land features have no effect on the groundwater flow.

The position of the top surface of the Friars Formation, illustrated in Figure A-5, is based on borehole data where the formation has been encountered in 43 wells. In addition, three geological cross sections in the proximity of Qualcomm Stadium have been used to infer the contact between the alluvium and the Friars Formation: 1) Cross Section C-C' (Plate 2A); 2) Cross Section B-B' (Plate 3B) (California Department of Conservation, Division of Mines and Geology, 2001); and 3) Section H-H' (California Department of Water Resources, 1965, Plate 4B). Site-specific data defining the base of the Friars Formation are not available. However, cross sections from geological maps (Plate 2A - La Jolla and Plate 3B - La Mesa quadrangle maps) show that the Friars Formation is at least 25 feet thick in the vicinity of the model domain. Consequently, a 25-foot uniform layer thickness was assigned to the Friars Formation throughout the model.

Several subtle changes have been made to the base of the original model. In general, the Friars Formation has been encountered in several boreholes drilled since 1999, indicating that the Friars Formation is deeper than was represented in the previous model. In the absence of current data, the previous model exhibits a bowl-like shape, deepest at the confluence of the San Diego River and the Murphy Canyon Creek. Recent borehole data suggest that each stream entering Mission Valley may be bedded in its own erosional trough with a gentle rise of the Friars Formation between streams (for example, at location of monitoring well cluster R-41). On the south side of the San Diego River, data indicating the depth to bedrock are very scarce. A U-shaped valley has been assumed, based on the available geological cross sections.

In DYN, layers are numbered from bottom to top. Layer 1, located at the base of the model, is composed entirely of Friars Formation with a uniform thickness of 25 feet. Layers 2

through 6 are composed of saturated alluvium. Geologic Indicator Kriging (GIK), the methodology for assigning lithology to the model cells, is described in Section A-2.0. Layer 7, located at the top of the model, is composed of unsaturated alluvium and fill. The top of Layer 7 is the topographic land surface. The thicknesses of the seven layers are interpolated equally for every vertical column of elements.

A-1.6 Boundary Conditions

Water enters the model domain as either atmospheric recharge or steam flow, particularly within the San Diego River and Murphy Canyon Creek. Water leaves the model through a specified head boundary on the western (downgradient) edge of the model domain. Gradually sloping fixed heads were specified across the width of Mission Valley, as used in the previous model, and were mirrored onto the southern side of the valley, south of the San Diego River. Figure A-6 illustrates the grid domain, fixed head nodes, and river nodes. The lowest specified head in the model is where San Diego River leaves the model domain. The head at this location equals the river stage and is fixed at 29 feet above mean sea level. This water level honors the stream bed elevation from FEMA Flood Insurance Studies (FIS) where the bridges of Freeways 805 and 163 cross the San Diego River. Variation in the specified head values of up to 5 feet have little effect on simulated flow conditions in the Terminal/Stadium area, due to the distance (approximately 11,000 feet) between the boundary and the Terminal/Stadium area.

Recharge data have been supplemented by information from the Turf Manager at Qualcomm Stadium. Figure A-7 illustrates the aerial distribution of recharge. Table A-2 summarizes the recharge parameters at the Qualcomm Stadium. The applied application rates for the playing field, the sod farm, and the practice field are 44.9 inches per year (in/yr), 23.0 in/yr, and 13.1 in/yr, respectively. This information was added to the recharge data file. Further refinement was made to the mesa-front recharge as used in the previous model. Higher rates of recharge were assigned to model nodes at the valley edge to represent inflow from adjacent upland areas. To assign rates of mesa-front recharge, the contributing watershed to the San Diego River valley and to Murphy Canyon was subdivided into sub-watershed areas. The upland area of each sub-watershed was multiplied by a rate of 2 in/yr to calculate the contribution to groundwater from each sub-watershed. The same procedure was used to determine the amount of mesa-front recharge from south of the San Diego River. The amount of applied mesa-front recharge ranged from 3 to 100 in/yr, with a median of 20 in/yr.

Table A-2: Summary of Recharge Parameters

	Irrigation Volume	Footprint	Application Rate	Net Recharge
Playing Field	8.6 ac.ft/yr	2.3 acre	44.9 in/yr	15.0 in/yr
Sod Farm/Practice Field	7.6 ac.ft./yr	4.0 acre	23.0 in/yr	7.6 in/yr
North Side Landscaping	7.7 ac.ft./yr	7.0 acre	13.1 in/yr	5.2 in/yr

ac.ft./yr = acre feet per year

New information on water infrastructure was obtained from the City and County of San Diego GIS department (SanGIS), specifically storm drain pipe layouts and sewer lines (Figure A-8). In some areas of the previous model, the mesa-front recharge was very high (up to 210 in/yr). Analysis of the GIS data revealed that several of these areas have storm drains that convey rain water to surface streams. One example is near the eastern flank of Murphy Canyon, where two 18-inch-diameter storm drains convey water from the surrounding urbanized mesa to Murphy Canyon Creek near Friars Road. Subsequently, the mesa-front recharge in this location was reduced to a more typical value of 35 in/yr.

The remainder of the alluvial valley was specified to be recharged by 3 in/yr in unpaved areas, and by 0.5 in/yr in the stadium parking lot and the maintenance yard southwest of the parking lot.

The same river boundary conditions have been used here as in the previous model, specifically for the San Diego River, Serra Mesa Creek, and Murphy Canyon Creek, including lined and unlined sections. The values of the streambed conductance were identical to those used to calibrate the previous model. These values correctly depict Murphy Canyon Creek as a losing stream, and the San Diego River as a gaining stream. No further refinement of streambed conductances was deemed necessary. The respective modeled streambed conductance values for the San Diego River, Murphy Canyon Creek, and Serra Mesa Creek are 2.5 square feet per day (ft^2/day), 1.65 ft^2/day, and 50 ft^2/day, respectively. In the steady-state calibration, both the San Diego River and Murphy Canyon Creek are assumed to carry an average water depth of 2 feet, while the creek from Serra Mesa is ephemeral. This is modeled by assigning a river boundary condition to every second node along the creek's trajectory. In transient calibrations, the water depth in the river was specified at 2 feet during a wet period, and was reduced to 1 foot during dry periods. The pumping boundary conditions for the two transient periods was the actual measured discharge from the five recovery wells, totaling 182 gpm from five recovery wells in August 2002 and 165 gpm from seven recovery wells in February 2003. Variation in evapotranspiration was not represented explicitly in the model. Seasonal changes in the riparian zone were deemed sufficiently addressed by the 1-foot changes in river stage.

A-1.7 Additional Features

Because recently collected data suggest that the MTBE plume is moving to middle or deep alluvial intervals as it migrates downgradient, a number of hydraulic features that may contribute to this phenomenon were added to the model. The drainage and dewatering systems near the stadium, landscape irrigation at the stadium, and storm-water drainage of the major roadways and its conveyance and/or retention were added (see Figure A-7 and Table A-2). The swale in the parking lot to the east of the stadium and the perimeter drain in the parking lot were added to evaluate potential influence on the groundwater balance and flow directions. Drain locations and leakage factors, water use, and irrigation patterns, together with updated recharge rates, were added to the model to improve the understanding of the groundwater flow system and the distribution of MTBE.

A-2.0 HYDROSTRATIGRAPHY

A-2.1 Geologic Indicator Kriging

To represent the lithologic characteristics in a more detailed manner than in the previous model, the lithology was interpolated between boreholes using a methodology for building three-dimensional geologic models based on indicator kriging, referred to Geologic Indicator Kriging (GIK). The GIK was conducted using Environmental Visualization System (EVS)-PRO software, developed by C Tech, Inc., of Huntington Beach, California. EVS kriging algorithms are based on the U.S. Environmental Protection Agency (USEPA) Geo-EAS geostatistical environmental assessment software (USEPA, 1991). Studies which have used indicator kriging to address hydrogeologic heterogeneities include Hsu et al. (1998); Varlien and Barcelona (1998); and Magowe and Carr (1999).

GIK addresses the complexities of the subsurface lithology by using and honoring data from all 5,480 feet of the 117 boring logs located within Mission Valley and Murphy Canyon. For cluster well locations, only the deepest boring log was counted and used. GIK evaluates every possible data pairing (over 50,000 per run) to generate a best-fit semivariogram in three dimensions, which in turn gives the distance-weighting factors for indicator kriging, which is then used to specify the most probable material in every cell of the GIK grid. Due to the high resolution of the DYN grid (25,144 nodes; 42,441 cells), interpolation of the GIK-assigned material groups into the DYN grid results in the ability to correlate the boring data with great accuracy.

A-2.2 Geologic Log Data Input

GIK relies on descriptions from geologic boring logs for input. Consecutive integer values (e.g., 1 through n, for n total observed material groups) are used to describe each material observed. Materials are numbered based upon the USCS soil classification system, as shown in Table A-3.

To build the GIK input files, for each boring, x, y, and z coordinates for the top and bottom of each lithologic interval, and the USCS soil type, were entered into a spreadsheet. This process was completed from geologic logs from 117 borings, for a total of approximately 5,480 feet of boring logs. A total of 844 discrete intervals were discerned in the GIK input file. For each boring, materials were assigned according to the USCS classification noted in the log for the depth intervals shown. The USCS classifications were grouped according to the following scheme, based on assumed similar hydraulic conductivities:

Table A-3. Geologic Indicator Kriging Material Assignments

GIK Material No.	GIK Group Name	USCS Classifications Included
1	Fill	-
2	Low K Alluvium	CL, ML

GIK Material No.	GIK Group Name	USCS Classifications Included
3	Medium K Alluvium	SC, SM
4	High K Alluvium	SP, SW, GC, GP,GW
5	Friars Formation	fine grained sandstone, occasionally SC

Figure A-9 illustrates an oblique, three-dimensional view of the soil borings in relation to the site map. Figure A-10 shows the soil borings in relation to a texture-mapped aerial photograph of the site.

The next sections describe how GIK is performed on the GIK grid, and how the resulting material types assigned to each GIK grid cell were interpolated onto the DYN computational grid. Each material type was subsequently assigned a uniform hydraulic conductivity value.

A-2.3 Description of GIK Gridding

EVS' GIK module, named *Indicator_Geology*, uses the thin plate indicator method for estimating surfaces from scattered data points. It assigns the geologic material cell data based on the nearest geologic material (in anisotropic space) as indicated in the boring log file. This is done based on the cell center coordinates and an enhanced refinement scheme for the borings. This method creates smooth surfaces that honor boring log data. The methodology creates layers of quadrilateral (4-node) elements in which each node is assigned the elevation for the specific geologic surface at that point in space.

A-2.4 Indicator Kriging Parameters and Settings

The EVS *Indicator_Geology* modules allow the user to control a full range of kriging parameters if desired. Alternatively, EVS's expert systems can be allowed to calculate and control parameters to minimize kriging variances. For the majority of GIK runs, the EVS expert system was allowed to control most parameters. The parameters and settings which were modified to evaluate various conditions for the indicator kriging runs are discussed below.

- The ***Semivariogram Symmetry*** parameter describes the degree to which EVS's expert system is allowed to distort the geometry of the semivariogram in calculating the best fit to the data. The valid range for this parameter is from 0 to 1. The default value is 1, which forces the semivariogram to be symmetrical in all axes of the data set. Unless the data being kriged shows a very high degree of asymmetry (direction-dependent correlation), good results are generally obtained by setting this parameter to a value between 0.5 and 1.

  The model area is located at the confluence of two fluvial systems with different orientations. Murphy Canyon is oriented generally north-south, and Mission Valley is

oriented generally east-west. Thus, depending on the location within the model area, it is possible that the principal direction of lithologic correlation may vary spatially from the north-south to the east-west. In order to evaluate whether variations in GIK-assigned material groups would result if semivariograms were aligned with Murphy Creek or the San Diego River, various scenarios were run with semivariogram symmetry ranging from 0.5 to 1, and the direction of the long axis ranging from 0 to 90 degrees. Results indicated that although variations in the semivariogram symmetry affect the uncertainty of the estimated material in each cell, the materials assigned to the cells by GIK are virtually identical in all cases due to the abundance of borings within the convex hull of the data domain. Because the intent of GIK was to populate the DYN model elements with the most likely material groups, the EVS expert system was allowed to select kriging parameters for the final GIK calculations.

- The ***Kriging Domain*** parameters allow the user to define the horizontal and vertical extent of the domain in which kriging of the parameter distribution will be completed. For the Mission Valley Terminal lithology, the GIK model was bounded by the convex hull defined by the boring log data set. Use of the convex hull was selected to confine indicator kriging to areas of the model where sufficient boring data exists. Areas outside the convex hull were assigned conductivity values in the DYN model based on calibration results. Figure A-11 illustrates the area bounded by the convex hull of the boring data, and the locations of the borings.

- The ***X / Y / Z Resolution*** parameters specify the number of grid nodes that will be included within the domain. The resolution used for the final GIK run was 51 X 51 X 36. GIK runs using finer grids extended computation times without resulting in appreciable changes in the material groups assigned to cells.

- The ***Horizontal/Vertical Anisotropy Ratio*** parameter allows the user to consider the effects of anisotropy in the material property represented by the indicator. The Horizontal/Vertical Anisotropy Ratio determines what multiplication factor will be used to apply biased weighting on data points in horizontal and vertical directions away from a given model node. A ratio of 10 was used, which allows data points in a horizontal direction away from a model node to influence the kriged value at that node 10 times more than data points an equal distance away in a vertical direction. Note that this anisotropy is a different property than the hydraulic conductivity anisotropy shown in Table A-4, Section A-3.2. The value of 10 was used for the lithology anisotropy ratio, as alluvium is deposited along generally horizontal surfaces, with the stream energy being the primary factor controlling the grain size of a given location. In contrast, the hydraulic conductivity anisotropy of material is related to the general deposition of particles on their flattest sides, and with the longest particle dimensions generally in line with the stream flow direction.

- The ***Pair Search Range*** specifies the radial distance from any input data point that will be searched to assemble the data pairs that are used in the variance analysis. The default value for the pair search range is set to 0, which results in the value being set to approximately $^2/_3$ of the largest distance between data points in the data set. The default value resulted in a range of 2,346 feet. EVS implements a deterministic random pair

selection algorithm to limit the total number of pairs that are considered in the semivariogram production when the number of potential pairs exceeds 50,000. Because the number of potential pairs of lithology combinations from the borings exceeded 50,000, the deterministic random pair selection algorithm was utilized.

A-2.4.1 Mapping GIK Results to the DYN Computational Grid

After GIK had been performed in EVS, the resulting material groups assigned to each GIK grid cell were interpolated onto the DYN model grid using the EVS *Interp_cell_data* module. The hydraulic conductivities for each material group type were assigned in DYN based on calibration runs.

Illustrations of the GIK results filtered by material types are shown in Figures A-12 through A-15. Illustrations of the GIK results filtered by DYN model layers are shown in Figures A-17 through A-21. An illustration including DYN layers 1 through 7 is not shown to avoid redundancy; it is identical to Figure A-16. Figure A-22 shows an example of the GIK material types as assigned to the DYN computational grid. Figure A-23 is an example illustration of a transect cross section in DYN showing several wells and the imported GIK material types.

A-2.4.2 Observations and Comparisons

The MVT conceptual model includes a coarser-grained sequence of sediments (basal gravel) overlying the Friars Formation as a predominant unit affecting groundwater flow and transport. The GIK-interpolated material types are consistent with this conceptualization, and illustrate the predominance of High-K alluvium (basal gravel) in DYN layers 2 and 3, and a generally fining-upward sequence in DYN layers 4, 5, and 6.

The occurrence of High-K alluvium in DYN layers 2 and 3, above the Friars Formation, is also consistent with differences in the response in the shallow and deeper portions of the aquifer observed during pumping tests (LFR 2002c).

In general, the GIK results do not indicate extensive region(s) of fine-grained material in the pathway of the plume. This is consistent with the boring logs and the existing plume geometry.

Close inspection of the GIK results illustrates a layer of relatively fine-grained silt/clay material near top of the saturated zone (DYN Layer 6) in the residual LNAPL area. Because this feature is in the LNAPL smear zone, it will likely affect source zone longevity.

A-3.0 MODEL SIMULATIONS

A-3.1 Calibration

Over 2,400 water level observations at more than 400 monitoring locations are currently available. The bulk of this data cover a 10-year time period and are sufficient to discern gradients, trends, and fluctuations. The previous model used river bed conductance, elevation, and stage as the key calibration parameters. These parameters were not altered in the present model. As an initial calibration step, data from pumping tests at RW-5 and RW-7 in July 2002 were matched using short-duration transient simulations. Here, the initial time step was taken at 0.07 day (100 minutes), and drawdowns were calculated at nodes corresponding to monitoring wells near the pumping wells. The maximum drawdown after two days of pumping was within 0.5 foot of the observed values. The aquifer test at RW-3 was not used for calibration because of its short duration (less than 5 hours) and minimal observed drawdown (0.3 foot). Calibration to recovery data was also performed and judged to be more reliable because the recovery data was not subject to well borehole storage effects. The recovery was observed during a two-day shut down of all recovery wells prior to the pumping tests. Figures A-24 and A-25 illustrate observed vs. simulated water level recovery for observation wells R-32 and R-34, respectively. In both wells the match improves noticeably after 1,000 minutes. The over-prediction of recovery in the early stages is probably due to water storage in the gravel pack, which has not attained steady-state after two days of pumping.

Water level hydrographs are shown in Figures A-26, A-27, and A-28. Figure A-26 shows hydrographs for wells in Murphy Canyon. Figure A-27 illustrates hydrographs for wells in the capture zone of the remedial pumping wells. Figure A-28 illustrates hydrographs for wells near the San Diego River. The water level hydrographs illustrate the cyclical, seasonal variations in water levels in the model area.

To further calibrate the model, two transient scenarios were selected using quarterly monitoring events representative of seasonal high and low groundwater levels. The February 2003 event was chosen as representative of the high seasonal water level conditions, and the August 2002 event was chosen as representative of the low water level conditions. These periods were chosen because they exhibit the largest differences between recent high and low water levels, and because these two time periods include most of the recently installed wells.

The high groundwater level scenario is represented in DYNFLOW by increasing recharge using a multiplier of 1.5. This adds 2 inches per year to the steady state scenario average recharge of 3.9 in/yr. The water depths in San Diego River and Murphy Canyon Creek are assumed to be 2 feet. The low groundwater elevation scenario is represented by zero recharge and a water depth of 1 foot in San Diego River. Each stress period is assumed to last 2 months.

Figure A-29 presents a calibration plot of observed vs. simulated water levels for all wells for the high water level scenario. Figure A-30 shows the calibration plot of observed vs.

simulated water levels in all wells for the low water level scenario. The data sets for Figures A-29 and A-30 were grouped by DYN model layer so that if variances were significantly large in a particular model layer, they would be easily identifiable. These plots also illustrate the groupings in particular regions of the site by elevation (e.g., Murphy Canyon, between Friars Road and San Diego Mission Road, the stadium vicinity, and near the San Diego River. The figures also show ideal calibration lines, and +/-5% lines to assist in evaluating goodness-of-fit. In general, simulated water levels are within ±5% of the ideal calibration line. In addition, the goodness-of-fit is similar for each model layer and location, indicating no apparent spatial bias in calibration. Figures A-31 to A-34 show the corresponding calibration metrics in terms of mean difference, standard deviation by model layer. The cumulative mean difference between observed and simulated head in all model layers was -0.014 foot for the August 2002 run, and -0.097 foot for the February 2003 period. These low values indicate minimal bias in the transient calibration.

Maps of the difference between observed and simulated water levels were generated as an additional method for evaluating the calibration results. Figures A-31 through A-34 illustrate delta observed-simulated water level maps for the low and high water level calibration scenario events. Figure A-31 shows the differences in water levels in the vicinity of the five pumping recovery wells for the low water level scenario event (August 2002). Figure A-32 illustrates the water levels in the shallow alluvium for the low water level scenario event. Figure A-33 shows the differences in water levels in the vicinity of the seven pumping recovery wells for the high water level scenario event (February 2003). Figure A-34 illustrates the water levels in the shallow alluvium for the high water level scenario. These figures indicate good model calibration over various regions of the site with standard deviations around 1.5 feet, while the water elevations across the model domain range over 60 feet.

Figure A-35 shows a cross-section in the direction of the general flow line from the Stadium to San Diego River. Scaled velocity vectors are plotted in each layer to illustrate the vertical flow component. For the wet calibration period (February 2003), the differences in water elevation between alluvium and the Friars Formation are in the order of 0.5 foot: downward between wells R-27 and R-26, and upward between wells R-26 and R-28. Wells north of the river exhibit upward gradients, with water level difference between AM and FS wells in the range from 0.14 (R-26) to 0.69 (R-24), indicating that the specified hydraulic conductivity for the Friars Formation is reasonable.

A-3.2 Calibrated Hydraulic Properties

The simulated areal distribution of aquifer materials has been illustrated in the GIK analysis. The calibrated hydraulic properties used for these materials are shown in Table A-4.

Table A-4: Calibrated Hydraulic Properties

Material Group	Horizontal Hydraulic Conductivity K_x	Horizontal Hydraulic Conductivity K_y	Vertical Hydraulic Conductivity K_z	Specific Storativity S_s	Specific Yield S_y
	ft/d	ft/d	ft/d	ft^{-1}	unitless
High K	150	150	75	0.00002	0.28
Medium K	50	50	25	0.00002	0.28
Low K	20	20	4	0.00002	0.28
Friars Fm	1	1	0.5	0.00002	0.05

K is the hydraulic conductivity (L/T), S_s is the specific storativity (in units ft^{-1}), and S_y is the specific yield. The storage terms for specific storativity, which represents elastic storage, are calculated from the dimensionless storativity as derived from the aquifer tests, divided by the aquifer thickness. Specific storativity is the volume of water released from storage per unit volume per unit head change. Specific yield (dimensionless) is the drainable yield at the water table, which is less than effective porosity, which in turn is less than the total porosity.

A-3.3 Validation

Several validation runs of the model were performed to evaluate the response of the model to different stresses. First, the recharge (including mesa-front recharge) was set to zero to simulate a prolonged drought. The model showed Murphy Canyon Creek losing all its surface water and the groundwater discharge to the San Diego River diminishing to near zero within the model area. The water levels dropped between 2 to 5 feet and the largest drop occurred at the upstream end of Murphy Canyon. This is correctly simulating a drought which progressively stresses a catchment from the higher stages down. The 2- to 5-foot drop corresponds well with seasonal variations observed in the groundwater elevations, which show a somewhat cyclic pattern with highs from April to September and lows from October to March. Another validation test was performed for a hypothetical 1-year pumping test scenario at RW-7. The calculated drawdown for the stressed aquifer system is greatest near the "neck" of Murphy Canyon. This is the area where the aquifer is the thinnest and the model correctly extends the cone of depression into the canyon.

A check was also performed on the regional water balance. The median stream flow for the San Diego River is 7.1 cubic feet per second (cfs) or 613,440 cubic feet per day (cfd). In the model, the San Diego River gains, under steady state conditions, 36,872 cfd as perennial flow. This translates to 6% of the total river flow as originating from the model area. The flowing length of the San Diego River is 26 miles. While there is no direct relationship between stream length and discharge, it is reasonable to assume that along the

2-mile stretch that is modeled, or 7.7% of its length, the contributing flow amounts to 6% of the total river flow.

The convergence criterion for the numerical solution was set at 0.05 foot. Iterations were continued until the maximum error at any node was less than this tolerance. The steady-state simulations converged after approximately 150 iterations and subsequent transient runs required 50 iterations per time step. The water balance closure was deemed adequate when inflows matched outflows and change in storage to within 0.5% at each time step. This is a typical amount of error due to rejected recharge, for example, if recharge flux is specified onto a fixed head or a river node.

A-3.4 Mass Balance

Table A-5 presents the mass balance summary, in units of cfd and gpm, for the calibrated steady-state model. The mass fluxes represent the total of the seven model layers and the simulation does not include remedial pumping. These fluxes are consistent with the fluxes from the previous steady-state model, with proportional increase in the model area (from 1.2 square miles to 2.1 square miles).

Table A-5: Summary of Water Mass Balance

Boundary	Inflow (cfd / gpm)	Outflow (cfd / gpm)
Surface Water		
San Diego River		24,940 / 129.6
Murphy Canyon Creek	17,769 / 92.3	
Serra Mesa Creek	800 / 4.2	
Recharge		
Aerial	28,127 / 146.1	
Mesa Front	27,139 / 141.0	
Western Model Boundary		48,896 / 254.0
Total	73,835 / 383.6	73,836 / 383.6

Notes: cfd = cubic feet per day
gpm = gallons per minute

A-3.5 Transport Modeling

A-3.5.1 DYNTRACK Program

Mass transport was simulated at the Mission Valley Terminal with DYNTRACK, a computer program for the simulation of three-dimensional contaminant transport. It is the companion code for DYNFLOW, a three-dimensional groundwater flow simulation code.

DYNTRACK uses the same three-dimensional finite element grid representation of aquifer geometry, flow field, and stratigraphy used in the DYNFLOW model. DYNTRACK can perform simple advective particle tracking, and can simulate three-dimensional reactive transport subject to first-order transformation, adsorption, and dispersion.

The DYNTRACK model simulates contaminant migration via the "random walk" particle tracking method, using a statistically significant number of discrete particles, each particle representing an associated contaminant mass, transformation rate, and retardation factor. Constituent concentration at any location and time is computed from the particle distribution as the total local particle mass divided by the water volume in which the local particles currently reside. Dispersion is simulated by imparting a random deflection to each particle in each time step. The magnitude and direction of the random deflection is controlled by the coefficients of dispersion.

DYNTRACK simulates the movement of dissolved contaminants in the saturated zone of the aquifer. Thus, neither migration of NAPL nor unsaturated zone transport can be simulated. Particle tracking is a Lagrangian approach (moving reference frame) in which the variation in space and in time of a fixed mass of contaminant is analyzed. This can be contrasted with an Eulerian approach (fixed reference frame) in which a continuous contaminant field evolves from a simplified source geometry. An advantage of the Lagrangian solution is that it inherently conserves mass, provided that all particles (i.e., discrete parcels of contaminant) are accounted for at the end of each simulation. Another advantage is that numerical dispersion, if any occurs, is not carried forward in time, because the solution algorithm does not depend on concentration at the previous time, as is the case with Eulerian algorithms.

While several other advantages of the random-walk particle tracking method exist, there are some potential disadvantages. The disadvantages stem from the random noise present in the solution, which increases as the number of particles decreases. A certain amount of random noise will always be present, regardless of the mesh density and the number of particles used. Direct computation of concentration from particle distributions often leads to irregular patterns of concentration contours, which are not aesthetically pleasing and may be difficult to interpret. Another disadvantage of the method is that there are no generally accepted criteria for selecting the number of particles. Trial-and-error tests using experience and judgment are required to determine if a solution is sufficiently accurate. The number of particles in these calculations was chosen such that the total number of particles within the plume was above 30,000 at all times.

A-3.5.2 Transport Modeling Approach

Groundwater flow conditions in the off-site areas of Mission Valley Terminal have changed over time due to alternating pumping schemes. Three different stress periods were identified to represent these transient conditions. The first period is a quasi-steady state starting in January 1991 and ending in May 1994, when the first remedial pumping started. This three-year period very closely approaches a steady state, with groundwater levels stabilizing with respect to the influences of river stage, areal recharge, and mesa-front

recharge. The next stress period spans 1994 to 2002, when five recovery wells were pumping intermittently to the northeast of the stadium (RW-3 to RW-7). Treatment system interruptions were simulated as variations in extraction rates, if the duration of the interruption was longer than the model time step of 30 days. The third stress period simulates a seven-well remedial pumping system with the addition of RW-8 (due north of the stadium) and RW-9 (near the western stadium entrance). Over the period from 1991 to 2010, the effects of the actual and projected remedial pumping are predicted by the model to draw down the water level underneath the stadium by 3.5 feet. Flow and transport calibrations were performed for the first and second stress periods, while the last period was used for prediction. Here, the predictive simulations seek to evaluate the effects of remedial extraction, estimate trends in future mass fluxes downgradient of the extraction system, and evaluate a range of possible outcomes of exposure point concentrations to future receptors.

The initial concentration of the residual LNAPL source and timing is unknown, as MTBE was present when chemical analysis for MTBE began in 1996. In 1991, however, LNAPL was observed in a cluster of off-site wells. Based on data from the existing wells, the residual LNAPL source was delineated and assumed to represent a "1991 source." It is approximated by a circle encompassing three persistent LNAPL wells T-2, T-21, and R-10. The area of this source is 112,280 square feet, or 2.6 acres. The initial strength of the source was taken at 110 milligrams per liter (mg/l), based on the highest concentration MTBE detected in groundwater at the Mission Valley Terminal (well S-1, sampled on July 8, 1999). In water, the reported solubility of pure MTBE is around 50,000 mg/l. In fresh reformulated gasoline, MTBE comprises 10 to 15% of the gasoline mixture. Therefore, no more than 500 to 750 mg/l is expected in groundwater near a fresh, undepleted source. Observations of this magnitude are uncommon.

The source strength was allowed to exponentially decay, from 110,000 parts per billion (ppb; equivalent to µg/l) in 1991 to 55 ppb in 2010. An exponentially declining source strength is based on observations in wells within the source area, particularly the MTBE concentration trends in wells R-12 and R-10. If no remedial pumping and no degradation had occurred, the total mass of MTBE remaining in groundwater in the model at the end of the 20-year period would be 88 kg. With the remedial pumping and assuming no degradation, only 7 kg MTBE is predicted to remain in the plume in year 2010. This simplified source was placed at the mouth of the Murphy Canyon and allowed flow with the simulated flow field. Figure A-36 shows a predicted particle track originating from that source and reaching the San Diego River in 20 years. This simulation assumed a steady-state flow field, no dispersivity, and no pumping. Processes that attenuate the plume such as biodegradation, dispersivity, and remedial pumping were considered in the following plume simulations.

The numerical transport model was used to simulate transport with and without the effects of biodegradation of dissolved MTBE; both cases assumed the same source strength; in the degradation case the dissolved mass in the plume was allowed to biodegrade according to a first-order transformation rate. A satisfactory match between simulated and observed MTBE concentrations could not be achieved with a single transformation rate over the entire simulation period. The simulation was therefore divided into two periods, from 1991

to 2001, and from 2002 to 2010. Best match was achieved with an initial transformation constant of 0.0005 d^{-1}, corresponding to a MTBE half-life of 1,386 days, and an increased transformation rate of 0.009 d^{-1} (half-life of 70 days) effective from 2002 to 2010. Both these values are in the range of literature values ranging from 60 days to 2,600 days (USEPA, 2000). Different hypotheses may explain why the apparent transformation rate increased by over an order of magnitude near the end of 2001:

- Remedial pumping may have changed the flow field in the downgradient portions of the plume such that groundwater containing greater amounts of dissolved oxygen and other electron acceptors began to enter into the flanks of the plume, favorably affecting the plume biodegradation.

- Extraction well RW-9, located along the apparent axis of the plume, began pumping in February 2003, which may have significantly changed the flow field, thereby pulling in more uncontaminated groundwater from mesa-front recharge north of the plume.

- There may be a lag time for MTBE biodegradation processes to start, as microbes need time to adapt to an unfamiliar carbon source or to new geochemical conditions resulting from changes in remedial pumping rates and locations.

Note that the model simulates degradation of MTBE via a first order transformation rate. The model does not simulate the formation and subsequent degradation of potential transformation byproducts such as tertiary butyl alcohol (TBA).

The empirical mass flux calculations (LFR, 2003) show a decrease in mass flux through Transect 1 (well clusters R-21 and R-30) and Transect 2 (well clusters R-27, R25, and R-21) by two orders of magnitude in the period from May 2001 to November 2002. Numerical simulations based on the calibrated flow field cannot reproduce this mass flux reduction without degradation of MTBE. With degradation, using the dual rate constants, the numerical simulation is compared to the empirical flux calculations in Figure A-37. The total MTBE mass in the plume has also been used to match the simulations to the empirical observations. For two periods when intensive sampling took place (November 2002 and February 2003), observed concentrations were integrated over interpreted isoconcentration contour areas to estimate plume mass. These values were used to match the mass in the numerical simulations as shown on Figure A-38.

While matching the plume mass and mass flux at two points in time, DYNTRACK was used to track future migration of MTBE through the aquifer system and predict concentrations at discrete time intervals. The transport model was calibrated to overall plume appearance (length and width), onset of plume shrinking, and observed concentrations. Table A-6 lists the parameters related to dispersion as used in the DYNTRACK simulations that best fit the observations.

Table A-6: Parameter Values Related to Dispersion

Material Group	Longitudinal Dispersivity α_L	Transverse Dispersivity α_T	Vertical Dispersivity α_V	Effective Porosity n_e
	ft	ft	ft	unitless
High K	14	1	0.4	0.28
Medium K	70	7	0.6	0.28
Low K	98	10	0.8	0.28
Friars Fm	1	0.04	0.6	0.04

Where:

α_L = the longitudinal dispersivity (L)

α_T = the transverse dispersivity (L)

α_V = the vertical dispersivity (L)

n_e = effective porosity (dimensionless)

The first remedial pumping period was simulated from May 1994, with five wells operating at a total discharge of 125 gpm for seven months. A second short pumping period was simulated from September 1996 to December 1996, with a total discharge from the five wells at 150 gpm. The next pumping period was from August 1998 to August 2001. A shutdown of two months was followed by a fourth pumping period from October 2001 to December 2002, when the total discharge was 170 gpm. Figure A-39 shows the simulated piezometric head contours for December 2002 for the five-well pumping scenario. With the completion of RW-8 and RW-9, this flow field is predicted to change to the predicted head contours shown in Figure A-40.

A-3.5.3 Transport Modeling Results

Particle clouds were converted by means of their respective mass to isoconcentration contour maps. The simulated isoconcentration contours for May 2001 are shown on Figure A-41 together with the observed MTBE results from the second quarterly sampling in 2001. This sampling period provided first data from wells near San Diego River for which the concentrations are predicted reasonably well. The match between observed and simulated concentrations is even better near the source as seen from plume boundaries and concentration values. Well R-29, near the Highway 805 bridge, has not shown repeatable MTBE occurrence and is not considered to be part of the plume body. The 2001 scenario shows contaminant particles that originated from the 1991 source and migrated for three years with the steady-state flow field. Subsequently, remedial pumping was started with

five recovery wells. Intermittent operation and partial penetration of the aquifer appears to have allowed some contaminant mass to migrate beyond the line of recovery wells.

The simulated contaminant distribution 2003 is shown on Figure A-42. Further mass reduction and narrowing of the plume core was predicted through the installation of RW-8 and RW-9 north and west of the stadium. The overall mass of MTBE in the plume is less than in 2001 and in very good agreement with the empirical plume mass (500 kg MTBE, Figure A-38). The predicted plume simulated for 2010 is shown on Figure A-43 when the plume is finally expected to fully detach from the region near the depleted source area and extraction wells. Numerous disconnections of the plume are shown, where MTBE persistence is typically associated low-K materials along the plume path. Note that some stagnation of MTBE concentrations (10 to 50 ppb) is shown to occur around pumping well RW-9. Stagnation points are occurring in this simulation because a quasi-steady flow field has developed where dissolved MTBE becomes caught within regions of near-zero hydraulic gradient. In reality, fluctuations in pumping rates and recharge will reduce the potential for stagnation.

A-3.6 Sensitivity Analysis

Sensitivity runs with DYNTRACK have shown that transformation rate and effective porosity are the most critical transport parameters. Transformation rate has been introduced to account for the sharp drop in observed concentrations throughout the plume, particularly since 2001, the year when almost continuous pumping from the remedial wells resumed. The observed plume mass dropped by 50% in a three-month period (from 701 kg MTBE in November 2002, to 331 kg in February 2003). Such a drop was not possible to numerically simulate through variation of the source mass or the flow field alone. A transformation rate constant of 0.0005 per day has been found to best match the plume mass from 1991 to 2001. A faster degradation rate with a rate constant of 0.009 per day was required to match the plume mass and empirical mass flux after 2001.

Porosity affects both the amount of water into which a contaminant mass is released and hence the concentration distribution, and the velocity components of flow and therefore mass flux. The effective porosity values used for alluvium (0.28) and for the Friars Formation (0.04) are in agreement with similar materials cited in literature. With biodegradation of MTBE, the simulated plume begins to shrink at the end of 2001, which is consistent with observation data. The arrival times of the plume front at monitoring well clusters R-21 and R-25 (inside and outside the west corner of the parking lot, respectively) were considered during calibration. The model predicts MTBE reaching R-21 in 1998 and R-25 in 1999. The first data available for R-21 are from February 2001, and the first data available for R-25 are from May 2001. MTBE was predicted to be present in the AM screened intervals of these wells, which indicates that the simulated plume is not migrating too slowly. The model predicts that MTBE will not reach R-29 (the westernmost monitoring well cluster, located near I-805), in the presence of biodegradation. This well has not shown any consistent occurrence of MTBE, indicating that the simulated plume is not migrating too quickly.

Another parameter adjusted during calibration was the transverse dispersivity. Simulations were verified for presence and absence of contaminants in monitoring wells located off the main axis of the plume. By adjusting the dispersivity, particles were able to reach areas to the south of the San Diego River, as has been observed in well cluster R-38. On the north side of the plume, predicted concentrations of MTBE in well R-20 remained non-detect at all times, which is supported by the field data. Despite reasonable appearance of the simulations over multiple years of observation data, the simulated plume extent does not match the observed plume extent at every monitoring point. For example, the model predictions show occurrence of MTBE beneath the stadium, which is not corroborated by the field data.

A-3.7 Numerical Mass Flux calculations

DYNTRACK calculates concentrations from the particle mass distribution at each time step by dividing the mass of particles by the volume of water in each grid cell. Each particle was given a weight of 353,357 units. This is a convenient conversion factor converting micrograms per liter to mass units per cubic foot. Particle release at a constant concentration source adds particles at each time step such that the concentration equals the specified value. The particles are then randomly input in each source cell in proportion to the weighted square root of the dispersion coefficient. In this way more particles are added to the source cells with higher velocities and/or volumes.

DYNTRACK automatically calculates cumulative mass profiles for each contaminant source and sink term, where the source is the fixed concentration boundary condition (with an exponentially decaying strength over time), and the sink terms are the remedial extraction wells, the riverbed discharge nodes, and at model boundary nodes. To calculate mass flux across transects drawn within the model domain, an artificial boundary of nodes following the two transects had to be construed. At the time steps for which output was desired (once a year) these transect nodes were given a fixed concentration of zero and the simulation was advanced for one additional time step (30 days). The mass flux was then calculated from number of particles removed from the model domain at the transect nodes as the closing term in the resulting mass balance. Because particles were effectively removed from the model, each subsequent mass flux simulation had to be recalculated.

The resulting mass flux calculations for Transects 1 and 2 are shown together with the empirical mass flux on Figure A-37. The timing of mass peaking and mass flux values are in reasonable agreement between the numerical and empirical results. Striking, however, is the width of the peaks as the mass passes through the transects. The numerical simulation predicts mass to pass through Transect 2 in approximately four years, while the empirical results shows the mass gone in one year. The width of the mass flux peak is dependent primarily on the flow velocity through the transect. A faster flow velocity in the numerical model was not possible to reconcile with the hydraulic property values from the calibrated flow model. One possible explanation is that only a narrow conduit has a very high hydraulic conductivity and transmits bulk of the contamination. More likely, however, is that the crude nature of the monitoring transects (consisting of two and three well nests,

respectively) missed the oncoming mass and started registering the plume only after May 2001.

A-3.8 Hypothetical Municipal Well Simulation

To investigate potential impacts on future potable uses of groundwater in the vicinity of the plume, a hypothetical supply well was simulated, producing 200 gpm beginning in January 2010. Based on hydraulic considerations, such a well is likely to be screened over as much saturated alluvium as possible, without having to drill too deep below sea level. These criteria were used to locate such a hypothetical well near monitoring well cluster R-26, which is 300 feet north of the San Diego River and close to the axis of the alluvial valley. Well cluster R-26 lies within the current MTBE plume.

To predict the concentration of MTBE in such a well, the DYNFLOW model was run as a transient simulation to generate a flow field under the influence of pumping from the hypothetical supply well. For this simulation, the remedial wells RW-3 to RW-9 are assumed to stop operating in January 2010. Figure A-44 shows the groundwater elevation contours after five years of pumping at a rate of 200 gpm from the hypothetical supply well. The cone of depression intersects with the San Diego River, indicating that the river will be losing water along its reach near this well. The resultant drawdown will also accelerate the movement of remaining MTBE mass toward the hypothetical pumping well.

Using the calibrated DYNTRACK model, simulations were made to predict MTBE concentrations in the water produced by the supply well (i.e., projected wellhead concentrations). To accomplish this, the predicted MTBE mass distribution for 2010 in the scenario with MTBE transformation was assumed to migrate under the influence of the newly generated flow field. The mass removed over time and the pumping rate were then used to calculate the concentration of MTBE in the produced water. Figure A-45 presents a time-series plot of simulated MTBE concentrations in a hypothetical supply well based on the particle-tracking simulation. As indicated on Figure A-45, MTBE concentrations below 0.2 µg/l will be present in the aquifer at that location in 2010. When the hypothetical supply well starts producing 200 gpm in 2010, groundwater from other portions of the plume will be drawn into the well. Depending on the location of MTBE in the 2010 plume, some hotspot remnants will require up to three years of travel time to reach the Hypothetical Pumping Well, as seen on Figure A-45 as a spike in 2013. The hypothetical simulation assumes the supply well intercepts the entire plume width and vertical extent of the alluvial aquifer, and is based on a conservative evaluation of mass flux that assumes dual-rate-degradation of dissolved-phase MTBE. Note that this simulation is an extrapolation of the present condition and that river stage, which will play a key role for such a production well, is assumed to remain constant. Actual river stage fluctuations, due to flood or drought, will have an effect on the MTBE time history at this location.

A-4.0 CONCLUSIONS AND RECOMMENDATIONS

The previous flow model has been expanded and recalibrated to simulate historical remedial pumping using five recovery wells, and current and future remedial pumping using seven recovery wells. Simulations of the operation of the five original recovery wells indicate that pumping-induced drawdown mainly affects the water levels in and near the Murphy Canyon. Simulations of the seven-well configuration indicate that some of the extracted water originates from the San Diego River, which will significantly increase the extent of hydraulic capture of the recovery system.

MTBE occurrences to the south of San Diego River have been simulated and calibrated, using the expanded model. By simulating MTBE releases to groundwater in the LNAPL area in the expanded model, the current magnitude and extent of MTBE downgradient of the LNAPL source area was reproduced. By using a random-walk dispersive particle tracking method, current occurrences of MTBE near the source and in the distal portions of the plume are adequately represented.

A simulated MTBE source centered around monitoring well T-18 with an initial concentration of 110 mg/l and an exponentially declining concentration results in a simulated plume that is consistent in occurrence, arrival times, and, in one of four transect calculations, with the observed mass flux passing though this plume. Such a source is estimated to have released a total of 8,700 kg of dissolved MTBE into the aquifer over a 20-year period.

Using the numerical transport model, these simulation results indicate that MTBE mass flux across Transect 1 drops from 280 g/day in 2000 to 0.06 g/day in 2010. If no biodegradation of dissolved MTBE is assumed, the simulated plume extent is much greater than observed, and results in a calculated mass flux of 1,000 g/day in 2000 and 89 g/day in 2010. With degradation, the transport model predicts that, in 2010, MTBE will remain in the lower permeability portions of the aquifer in concentrations of 10 to 42 ppb. Without degradation, the model predicts a coherent MTBE plume with maximum concentrations up to 1,700 ppb.

A hypothetical supply well was placed in this future plume configuration in the location of well R-26, and pumped at 200 gpm. At this location, the alluvium is sufficiently thick to sustain 200 gpm of production. In addition, more than half of the aquifer thickness is above mean sea level, and the resulting regional drawdown is not likely to exceed 3 feet during average recharge conditions. The model predicts that with biodegradation, maximum MTBE concentrations in such a well would be below 0.2 ppb. If the plume were not biodegrading, the model predicts that such a well could produce water containing MTBE concentrations near 20 µg/l during its first year of operation. These concentrations are predicted to gradually decrease after two years of pumping at a projected rate of 200 gpm.

The simulations indicate that water quality objectives would be achieved in a hypothetical supply well downgradient of the remedial extraction wells should the well begin pumping in the year 2010. This result assumes that MTBE continues to attenuate, even at a relatively low rate. If no biodegradation occurs, with the hypothetical pumping well beginning

operation in 2010, a 5 µg/l MTBE water quality objective in such a well would not be achieved until 2013.

A-5.0 REFERENCES

ASTM. 1993a. Standard Guide for Application of a Ground-Water Flow Model to a Site-Specific Problem. ASTM D5447-93.

_____. 1993b. Standard Guide for Comparing Ground-Water Flow Model Simulations to Site-Specific Information. ASTM D5490-93.

_____. 1995. Standard Guide for Documenting a Ground-Water Flow Model Application. ASTM D5718-95 (Reapproved 2000).

_____. 1996a. Standard Guide for Calibrating a Ground-Water Flow Model Application. ASTM D5981-96.

_____. 1996b. Standard Guide for Analysis of Spatial Variation in Geostatistical Site Investigations. ASTM D5922-96.

_____. 1996c. Standard Guide for Selection of Kriging Methods in Geostatistical Site Investigations. ASTM D5923-96.

California Department of Conservation, Division of Mines and Geology. 2001. Geology of the San Diego Metropolitan Area, California. Bulletin 200. Plate 2A - Geology of the La Jolla Quadrangle, San Diego County, California. Plate 3B - Geology of the La Mesa Quadrangle, San Diego County, California.

California Department of Water Resources. 1965. Ground Water Conditions in San Diego River Valley. Section H-H', Plate 4B. September.

California EPA. 1995. Ground Water Modeling for Hydrogeologic Characterization – Vol. 1 Field Investigation Manual. July.

California Regional Water Quality Control Board, San Diego Region. 1994. Water Quality Control Plan for the San Diego Basin.

Camp Dresser & McKee. 1999a. Technical Memorandum No. 5. Groundwater Modeling Documentation. SFPP, L.P., Mission Valley Terminal Remediation System Focused Feasibility Analysis and Implementation. September 20.

_____. 1999b. Mission Valley Terminal, Corrective Action Plan. October.

City of San Diego. 2002. Aerial photographs and topographic data obtained by Scott Martin of LFR.

Freeze, R. Allan, and John A. Cherry. 1979. *Groundwater*. Prentice-Hall, Inc.

Gastil, G., and R. Higley. 1977. Guide to San Diego Area Stratigraphy: Prepared for AAPG-SEG Petroleum Exploration School Field Trip. San Diego State. December.

Hsu, K.C., D. Jordan, T.N. Blandford, D.W. Reaber, and J.L. Wilson. 1998. Evaluation of a Local-Scale Contaminant Migration Within a Heterogeneous Alluvial Basin in the Southwest. AGWSE Technical Education Session: 1998 Abstract Book; Dealing with Hydrogeologic Heterogeneity: Resolutions to the Problem and Remaining Limitations, December 13-16, Las Vegas, NV; P149-150.

Kleinfelder. 2000. Preliminary Report of Findings, Mission Valley Terminal and QualComm Stadium. November 17.

_____. 2001a. Supplemental Groundwater Assessment, Mission Valley Terminal. February 26.

_____. 2001b. Interim Groundwater Assessment, Mission Valley Terminal. San Diego, California. June 29.

_____. 2002a. Interim Groundwater Assessment Report, Mission Valley Terminal. January 18.

_____. 2002b. Supplement to Interim Groundwater Assessment Report, Mission Valley Terminal. February 21.

LFR Levine·Fricke. 2002a. Work Plan for Groundwater and Contaminant Transport Modeling, Mission Valley Terminal, 9950 and 9966 San Diego Mission Road, San Diego, CA. Submitted to Kelly Dorsey, Water Quality Control Board, San Diego Region 9. June 10.

_____. 2002b. Monitoring Well Installation Report for 18 Wells at Qualcomm Stadium, 9449 Friars Road, San Diego, CA. August 7.

_____. 2002c. Quarterly Groundwater Monitoring Report, Third Quarter of 2002, Mission Valley Terminal, San Diego, California. October.

_____. 2002d. Groundwater Extraction Evaluation of Existing Recovery System, Mission Valley Terminal, San Diego, California. November.

_____. 2002e. Soil-Vapor Extraction System Evaluation. Mission Valley Terminal. San Diego, California. November 22.

_____. 2002f. Monitoring Well Installation Report for 8 Wells at Qualcomm Stadium, 9449 Friars Road, San Diego, CA. August 7.

_____. 2003a. Quarterly Groundwater Monitoring Report, Fourth Quarter of 2002, Mission Valley Terminal, San Diego, California. January.

_____. 2003b. Well Drilling Report for Groundwater Monitoring Wells R-43AS, R-43AD, R-44AS, R-44AM and R-44AD, QualComm Stadium, 9449 Friars Road, San Diego, CA. January 30.

_____. 2003c. Work Plan Update for Modifications to the Existing Soil-Vapor Extraction and Groundwater Extraction Systems, Mission Valley Terminal, San Diego, California. February.

_____. 2003d. Well Drilling Report for Groundwater Monitoring Wells R-45 through R-48, Qualcomm Stadium, 9449 Friars Road, San Diego, CA. April 1.

_____. 2003e. Quarterly Groundwater Monitoring Report. First Quarter of 2003. Mission Valley Terminal. San Diego, California. April 30.

Magowe, M. and J.R. Carr. 1999. Relationship Between Lineaments and Groundwater Occurrence in Western Botswana. Ground Water, v37 N2; P282-286. February.

TRC. 2000. Delineation of the Horizontal and Vertical Nature and Extent of Fuel Additives in Groundwater, Mission Valley Terminal. June 30.

USGS. 1996. Digital Elevation Model (DEM) for the La Jolla, CA, 7.5-minute quadrangle.

_____. 1998. Digital Elevation Model (DEM) for the La Mesa, CA, 7.5-minute quadrangle.

U.S. Environmental Protection Agency. 2000. Natural Attenuation of MTBE in the Subsurface under Methanogenic Conditions. Office of Research and Development, Cincinnati, OH 45268. EPA/600/R-00/006.

_____. 1993. Compilation of Ground-Water Models, Office of Research and Development, Washington DC 20460, EPA/600/R-93/118. May.

_____. 1991. Geo-EAS (Geostatistical Environmental Assessment Software) User's Guide. Evan J. Englund, U.S. EPA, and Allen R. Sparks, Computer Sciences Corporation. EPA Contract 68-01-7325.

Varljen, M.D. and M. Barcelona. 1998. Combining Adaptive Site Characterization and Probabilistic Approaches to Address Hydrogeologic Heterogeneity. AGWSE Technical Education Session: 1998 Abstract Book; Dealing with Hydrogeologic Heterogeneity: Resolutions to the Problem and Remaining Limitations, December 13-16, Las Vegas, NV; P92-93.

Wang, H.F. and M.P. Anderson. 1982. Introduction to Groundwater Modeling: Finite Difference and Finite Element Methods, W.H. Freeman and Co., 237 p. (REPRINTED, 1995) Academic Press, San Diego.